separations

MDPI

Article

Adsorption of Chromium (VI) from Aqueous Solution Using Palm Leaf-Derived Biochar: Kinetic and Isothermal Studies

Samah Daffalla [1,2]

[1] Department of Environment and Agricultural Natural Resources, College of Agricultural and Food Sciences, King Faisal University, P.O. Box 400, Al-Ahsa 31982, Saudi Arabia; sbalal@kfu.edu.sa
[2] Department of Chemical Engineering, College of Engineering, University of Khartoum, Khartoum P.O. Box 321, Sudan

Abstract: In this study, biochar produced by low-temperature pyrolysis from palm leaves was treated with phosphoric acid in order to increase the sorption efficiency of Cr (VI) from aqueous solutions. Numerous characterization experiments using BET surface area, FE-SEM and FT-IR showed that the phosphoric acid-treated biochar (TBC-P) was covered with P particles. In comparison to the palm leaves and biochar, the TBC-P also had more surface oxygenated functional groups, surface area, pore size and internal structure. FTIR analysis showed that the functional groups of pretreated biochar were similar to those of biochar. Batch adsorption experiments showed that the TBC-P had a strong sorption ability to Cr (VI), with the highest removal efficiency of 99% at a low pH value of 2.0, which was significantly higher than that of the untreated biochar. The kinetic study has shown that the mechanism of the reaction was well represented by the second-order model, while isotherm data were well presented by the Langmuir model. The TBC-P was successfully regenerated using a 0.1 M HCl solution.

Keywords: palm leaves; biochar; adsorption kinetics; adsorption isotherms; Cr (VI) removal

Citation: Daffalla, S. Adsorption of Chromium (VI) from Aqueous Solution Using Palm Leaf-Derived Biochar: Kinetic and Isothermal Studies. *Separations* **2023**, *10*, 260. https://doi.org/10.3390/separations10040260

Academic Editor: Hideo Maruyama

Received: 30 March 2023
Revised: 9 April 2023
Accepted: 12 April 2023
Published: 17 April 2023

1. Introduction

Biomass is obtained from organic material (plant and animal byproducts) and is available naturally. Different kinds of wastes such as sludge and various industrial wastes are also treated as biomass. Currently, biomass-based adsorbents are used for the removal of many contaminants from wastewater. These materials are eco-friendly, low-cost, and abundant. In addition, in the view of environmental preservation, the use of biomass can significantly mitigate global warming by reducing carbon [1–3]. Dates are a major crop in Saudi Arabia and are generated in huge amounts from date palm due to the presence of the date processing industry. As a result, thousands of tons of palm waste are produced yearly, and most of this waste is burned or discarded, causing pollution to the surrounding environment [4]. Thus, converting palm waste into high-value biochar products reduces the impact on the environment.

Biochar has great potential for the treatment of wastewater. Biochar can be manufactured from biomass using thermochemical technologies. However, the use of low-temperature pyrolysis is among the most effective thermochemical processing technology to extract biochar from biomass [1]. The manufacture of biochar through pyrolysis is affected by many parameters (i.e., temperature, reaction time, nitrogen flow and others). The above-mentioned parameters influence the yield and quality of the biochar. Moreover, the structure and content of the cellulose, hemicellulose and lignin in the biomass also influence the biochar yield [1,3,5]. The major components of date palm biomass are cellulose, hemicelluloses and lignin [4]. In addition, date palm has a low moisture content and a high volatile solids content, which influence the char yield and structure of the biochar.

Nowadays, heavy metal contamination has become one of the most significant environmental issues. Most of the heavy metals disposed of in wastewater are considered

toxic and carcinogenic to humans [6,7]. Hexavalent chromium, Cr (VI), is an acutely toxic metal for humans, causing carcinogenic and mutagenic effects. It is also toxic to animals and plants [8]. So far, numerous efficient methods have been reviewed for the removal of metals from wastewater, such as biological oxidation, coagulation, membrane separation and adsorption [9–13]. The adsorption process has been shown to be an effective and technically feasible process for metal uptake from aqueous solutions [11,12]. Metal removal from aqueous solutions by biochar derived from agricultural by-products has been studied by many researchers [14–16]. The biochar adsorbent developed from biomass through a low-temperature pyrolysis process for the adsorption of heavy metals is a simple operation that is environmentally friendly, has broad adaptability and supports both the circular economy and sustainability [17]. There are many methods that are used to modify biochar properties, such as using acids, alkalis, steam, metal oxides and organic compounds. These treatments had been proven to enhance the surface properties, porous structure, surface area, functional groups and performances of biochar, and thus increase its ability to remove metals from wastewater [18]. Acid treatments provide more oxygenated functional groups on biochar surfaces and increase the potential for biochar to chemically bind positively charged pollutants through specific adsorption. The chemical agent phosphoric acid (H_3PO_4) was chosen as the activation agent because it is less corrosive and less environmentally hazardous. It also has a higher chemical recovery efficiency than other agents. In particular, biochar modified with H_3PO_4 has been shown to enhance the adsorption capacity of Cr (VI) [19]. Phosphoric acid is indeed an effective chemical activator to improve the adsorption of biochar, not only by increasing the pore size and specific surface area but also by enhancing the adsorption of other ions on the functional groups' surface area [19]. The literature shows that different biochars, such as Artemisia argyi stem [5], banana peduncle [20], Acorus calamus Linn [21], wastewater hyacinth [22], peanut hull [23], mangosteen shells [24], Melia azedarach wood [25], peanut shell-derived biochar [26] and H_3PO_4-treated biochar [27], have been utilized to remove Cr (VI) from contaminated aqueous systems. Various studies had been performed previously by researchers for investigation on the pyrolysis of agricultural wastes and the use of the obtained biochar in different ways, but there is a gap in the use of biochar from waste palm leaves in the adsorption of heavy metals from wastewater. Further, in spite of Saudi Arabia producing large amounts of palm waste, not much research has been conducted on its use as an adsorbent for the various heavy metals that continuously harm the environment. To fill this research gap, this study was conducted to find out the best operating parameters for the effective adsorption of Cr (VI) onto biochar produced from palm leaves.

The objective of this work is to increase the metal-binding capacity of biochar produced from palm leaves by chemical modification using phosphoric acid. The characteristics of developed adsorbents were examined. Adsorption experiments were studied considering various contact times, adsorbent doses, initial metal concentrations and pH. The adsorption kinetics of Cr (VI) and isotherms were studied using various models.

2. Materials and Methods

2.1. Materials

The feedstock for the production of biochar was palm leaves collected from a farm in Al-Ahsa, Saudi Arabia. Palm leaves are generally one of three types: pinnate, palmate or costapalmate. The major constituents of palm leaves are cellulose, hemicellulose and lignin. In this study, the palm leaves were rinsed thoroughly using distilled water and dried at 70 °C for 24 h before pyrolysis. A total of 1000 mg/L Cr (VI) stock solution was set by dissolving an accurately weighed quantity of $K_2Cr_2O_7$ (molecular weight 294.18) in 1000 mL distilled water. A total of 0.1 M HCl and 0.1 M NaOH were used to control solution pH. Phosphoric acid (1 M H_3PO_4, Merck, Darmstadt, (Hesse), Germany) was used for chemical modification of biochar. All of the reagents were of analytical reagent grade.

2.2. Development and Characterization of Biochar

Untreated biochar (UBC) used in this study was developed by pyrolyzing ground palm leaves (PL) (sized between 250 and 125 µm) in a furnace at 600 °C for 1h with the absence of oxygen. After that, the developed biochar was modified using strong acids (1 M H_3PO_4) to increase the acidity of the surfaces and porous structure. For acid treatment, 5 g of the UBC was subsequently immersed in 200 mL solution with 1 M H_3PO_4 and stirred for 24 h. Then, the treated biochar was rinsed thoroughly with distilled water and dried at 70 °C for 24 h; the treated biochar was named TBC-P (Figure 1).

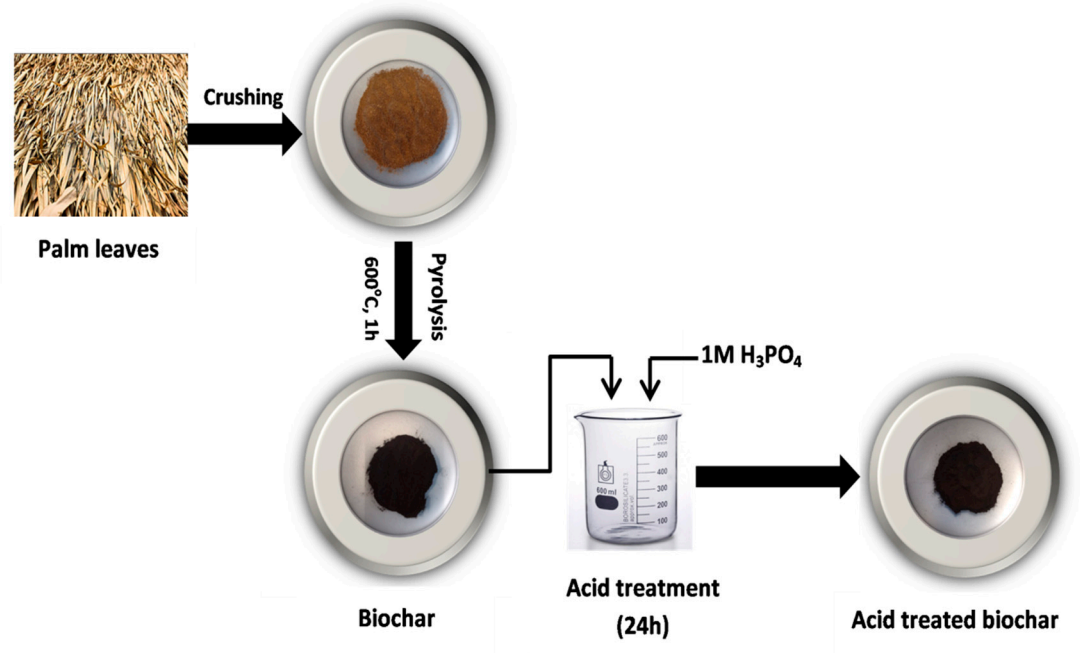

Figure 1. Schematic representation for the preparation of the TBC-P.

The morphology of palm leaves (PL) and developed biochar adsorbents (UBC and TBC-P) were characterized using field emission scanning electron microscopy (FE-SEM, model FEI, QUANTA FEG 250, Manufacturer, Redcar, (North East), United Kindom). The Brunauer–Emmett–Teller (BET) method was used for measurement of surface area using micromeritics (ASAP 2020). Fourier-transform infrared spectroscopy (FT-IR, Cary 630 FT-IR Spectrophotometer model, Manufacturer, Santa Clara, (California), United States) was used for FT-IR analysis.

2.3. Batch Adsorption

Batch studies were applied using elementary flask (100 mL) with 30 mL fixed initial concentrations of Cr (VI) solution. The effect of several parameters, including pH (2.0–8.0), initial metal concentration (10–250 mg/L) and adsorbent dose (0.005–0.2 g), and contact time was studied. The suspensions were separated using Whatman No.1 filter paper. The filtrate was used to determine the concentration of the Cr (VI) at wavelength of 367 nm using the UV-vis spectrophotometer (Shimadzu UV-1601, Kyoto, Japan). Kinetics were studied at initial metal concentration of 20 mg/L at 0.2 g adsorbent dose, pH 2.0, 25 °C and shaken at 120 rpm. The adsorption time was set to 2, 5, 10, 15, 20, 25, 30, 40, 50, 60, 80, 100 and 120 min. The metal removal efficiency and adsorption capacity were determined using Equations (1) and (2). All experiments were pending duplication as well as value averaging when analysis was performed.

$$\%\ \text{removal percentage of Cr (VI)} = \frac{(C_0 - C_t)}{C_0} \times 100 \quad (1)$$

$$\text{Amount Adsorbed } (q_e) = \frac{(C_0 - C_e)V}{W}, (\text{mg ofadsorbate/g of adsorbant}) \quad (2)$$

where C_0 and C_t (mg/L) are the initial Cr (VI) concentration and the Cr (VI) concentration at time t, respectively. C_e (mg/L) is the concentration of Cr (VI) at equilibrium, V is the volume (L) and W is the mass of used adsorbent (g).

3. Results and Discussion

3.1. Characterization of Adsorbent

At low temperatures and a low heating rate process, the yield value was 48.77% for UBC, which is acceptable in comparison to other research for some biochars developed from agricultural wastes [28].

3.1.1. FT-IR Analysis

The FT-IR analysis of feedstock and both developed biochars (UBC and TBC-P) is presented in Figure 2. The FT-IR spectra of adsorbents are displayed in Table 1. For palm leaves, the existence of bands at 328, 360, 2915, 1616, 1367, 1240, 1019, 875, 754 cm^{-1} was specified for functional groups, such as hydroxyls, olefins, esters and ethers (Figure 2) [29]. In contrast, as shown in Figure 2, the FT-IR bands of the UBC and TBC-P are comparable; however, the IR peak derived from C-O stretching of alcohols exhibited a relatively high IR intensity in the TBC-P compared to the UBC in the range of 1370–1200 cm^{-1} because the phosphoric acid pre-treatment promoted the formation of oxygen-containing functional groups. This was consistent with the findings of another study, which showed that carbonyl-containing groups formed or increased during the activated carbon modification process using H_3PO_4 [30]. The band at 1616 cm^{-1} in palm leaves explains alkenyl C=C stretching vibrations. This can also explain the H-O-H bending band of water, which tends to decrease after pyrolysis. The strong absorption bands between 3600 and 3400 cm^{-1} indicated the presence of amino and hydroxyl groups. Compared with other biochars, the palm leaves were associated with strong absorption bands at 3283 cm^{-1}, which correspond to hydroxyl or amino groups. It can be noticed that the pyrolyzed biochars and the feedstock have common functional groups, and the leaf feedstock was dehydrated upon pyrolysis [31]. Further, the content of hydroxyl, carboxyl and amino groups that are accountable for the sorption in the UBC and TBC-P biochars [29,31] was reduced compared to the feedstock, as shown in Figure 2.

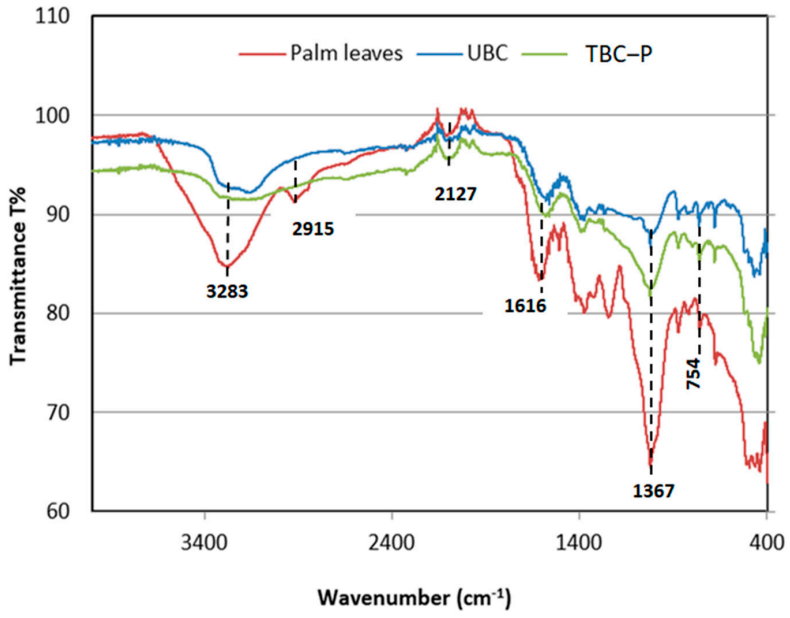

Figure 2. FTIR spectra of palm leaves, UBC and TBC-P.

Table 1. FT-IR functional groups on palm leaves, UBC and TBC-P adsorbent.

Wavenumber (cm^{-1})				Functional Groups
Reference	**Palm Leaves**	**UBC**	**TBC-P**	
3600–3400	3283	3376	3340	O-H Stretching of alcohol, carboxylic
3100–3000	2915	-	-	C-H Stretching of alkyne, benzene
2260–2100	2127	2149	2100	C-C Stretching of alkyne
1650–1600	1616	1620	1577	C=C Stretching of alkene
1300–1000	1367, 1240, 1019	1349, 1028	1373, 1020	C-O Stretching of ether, ester
1000–675	875, 754, 673	680, 463	678, 440	C=C, C-H Stretching of bending

3.1.2. FE-SEM Analysis

FE-SEM images of UBC and TBC-P biochars as well as feedstock are shown in Figure 3. This figure shows that the surface texture of the palm leaves was non-porous, rigid and densely formed (Figure 3a) [31]. In addition, the palm leaves had an integrated texture lacking significant pores, as compared to the developed biochars. In contrast, the pyrolyzed biochars (UBC and TBC-P) had a porous texture and smooth wall surfaces (Figure 3b,c). However, the number of pores increased in the TBC-P sample as the acid treatment separated the weakly bonded constituents on the UBC surface, which contributed to an increase in porosity (Figure 3c). Indeed, the porosity of biochar changes with feedstock type and pyrolysis circumstances.

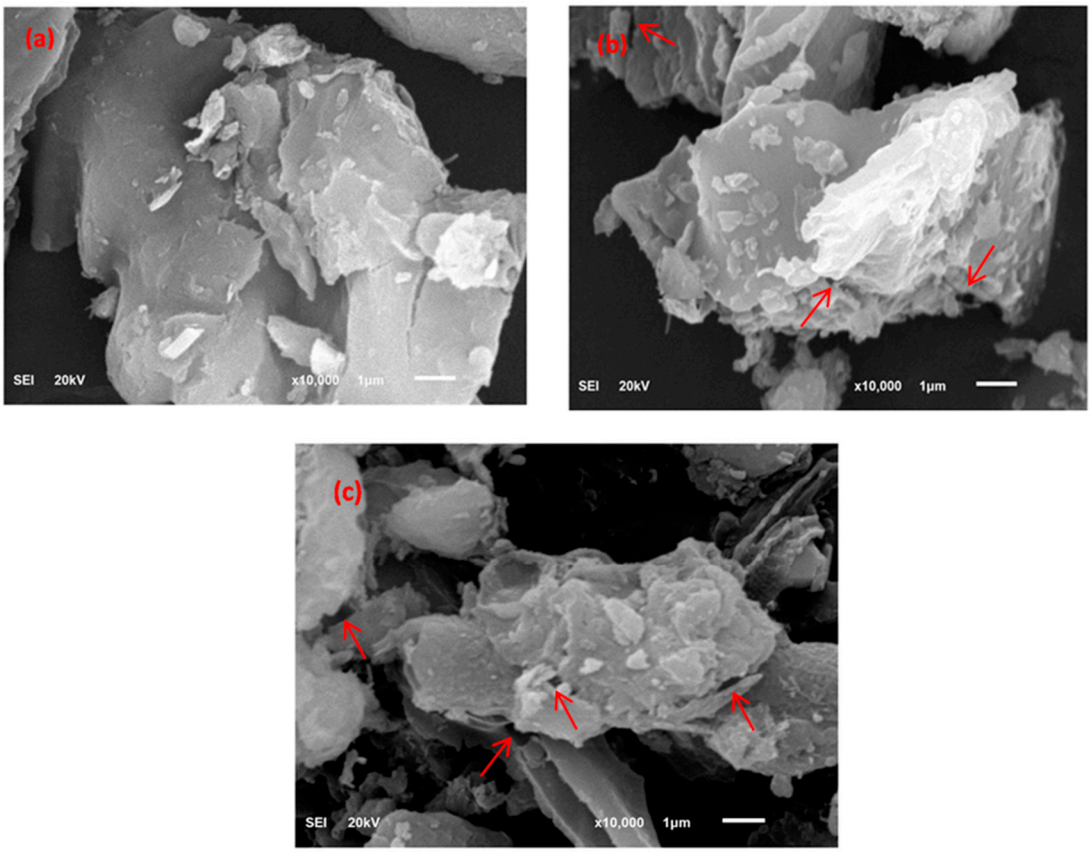

Figure 3. FE-SEM images of (**a**) palm leaves, (**b**) UBC and (**c**) TBC-P.

3.1.3. Surface Area Analysis

Figure 4 shows the hysteresis loops of palm leaves, UBC and TBC-P. According to the IUPAC classification, the palm leaves and UBC showed types II and IV with an H3 hysteresis loop, which is typical of mesoporous and macroporous structures [32], while the TBC-P adsorbent showed type IV isotherms with an H3 hysteresis loop, which is typical of mesoporous and microporous structures. Actually, when the pyrolysis temperature was more than 550 °C, the size of the mesopores increased and new micropores were formed [33]. Moreover, BET analysis revealed the fact that the palm leaves were characterized by a low surface area (2.03 m^2/g) and their acid-treated biochar showed the largest surface area (37 m^2/g) followed by the untreated biochar (12.7 m^2/g) (Table 2). A high surface area of TBC-P with a large distribution of mesopores indicates the suitability of the treatment procedure, which provides a large number of adsorption sites upon which pollutants can adsorb.

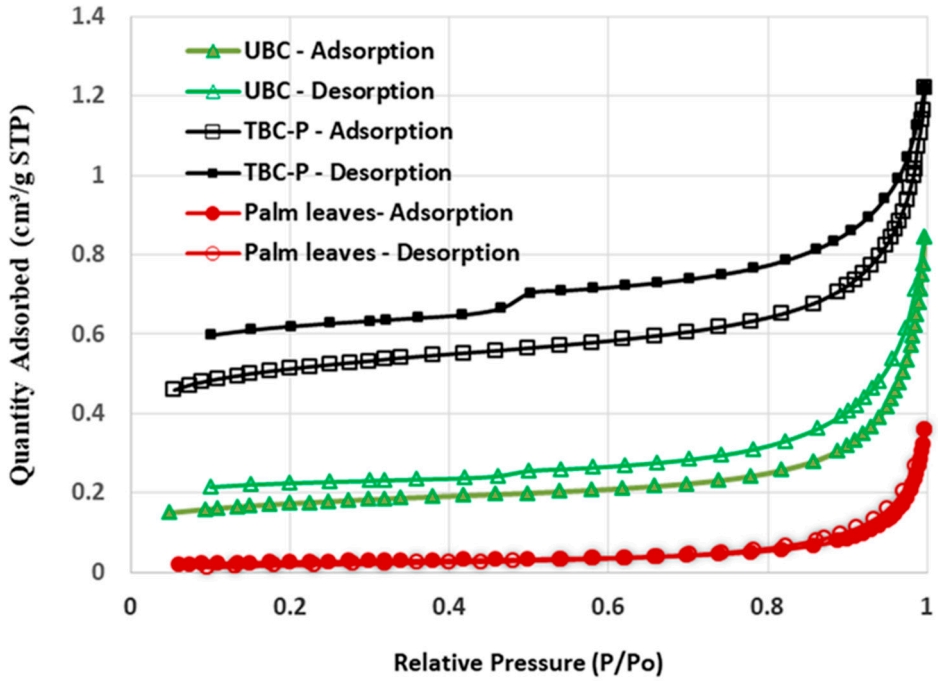

Figure 4. Hysteresis loops of palm leaves, UBC and TBC-P.

Table 2. Pore characteristics of palm leaves, UBC and TBC-P.

Adsorbent	BET Surface Area (m^2/g)	Total Pore Volume (cm^3/g)	Average Pore Diameter (nm)
Palm leaves	2.030	0.0106	25.91
UBC	12.71	0.0229	16.44
TBC-P	37.01	0.0279	9.16

The pore size distribution of palm leaves, UBC and TBC-P adsorbents is illustrated in Figure 5. It was found that palm leaves showed a relatively broad pore distribution, while the pore distribution changed into mesopore sizes, centered at 4 nm and 2.9 nm for the UBC and TBC-P samples, respectively. However, the mesopore volume of the TBC-P sample at 4 nm was larger than that of the UBC.

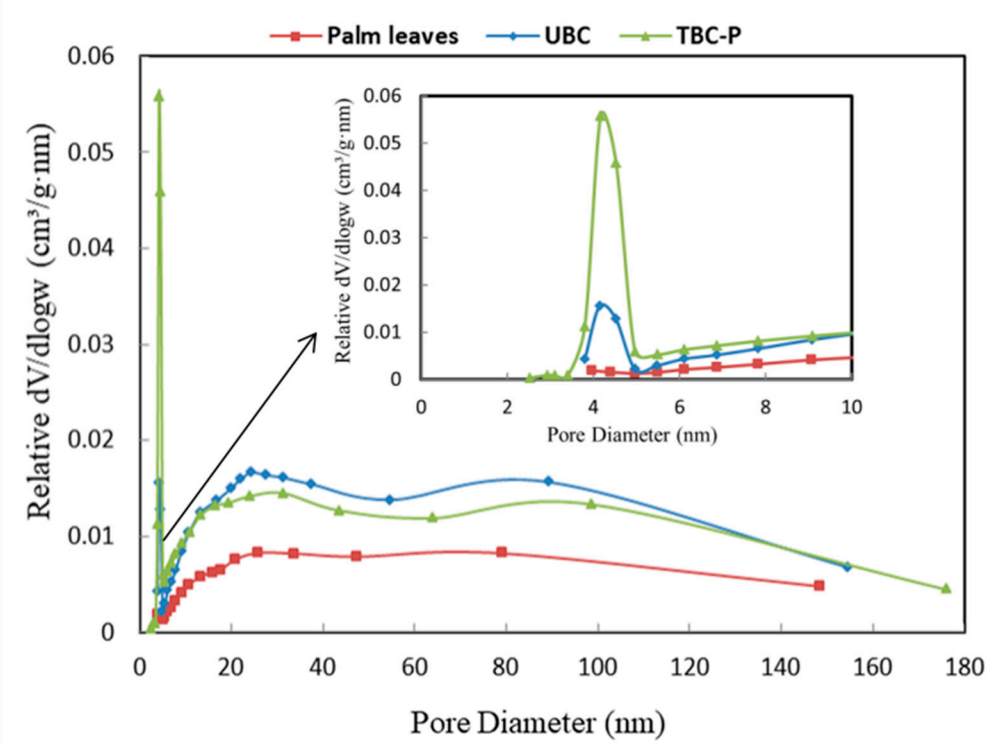

Figure 5. Pore size distribution of palm leaves, UBC and TBC-P.

3.2. Adsorption Studies of Cr (VI)

3.2.1. Effect of Adsorbent Type

Firstly, it was necessary to compare the removal efficiency of TBC-P with that of UBC and palm leaves: 0.2 g of each adsorbent was added to the 20 mg/L Cr (VI) solution at pH 2.0 and 25 °C for 24 h. The results revealed that the metal removal efficiency using TBC-P was 99%, while it was 61% and 85.9% for palm leaves and UBC, respectively. In this study, the surface area of TBC-P was measured at 37 m^2/g by a BET analyzer. The surface area of UBC-P was 18.2 times larger than the surface area of palm leaves and 2.9 times larger than UBC. The acid treatment of biochar with phosphoric acid improved the surface area and the total pore volume. The integration of P-O-P bonds into the carbon structure improved the Cr (VI) removal efficiency due to phosphate deposit and surface adsorption [29]. Surface area, porous structure and surface functionality influenced the uptake of Cr (VI) on the TBC-P [29]. Hence, the TBC-P was suggested for more studies.

3.2.2. Influence of Solution pH on Metal Uptake

The pH plays a vital role during adsorption since it affects the surface charges of the TBC-P sample and Cr (VI) uptake. Figure 6 depicts the effect of pH on the removal efficiency and adsorption capacity of Cr (VI) by TBC-P adsorbent. The influence of pH was carried out at pH ranging from 2 to 8, 20 mg/L initial metal concentration, 0.2 g adsorbent dose, 24 h of contact time and at ambient temperature (25 °C). From Figure 6, it is evident that the Cr (VI) sorption is highly pH-dependent, a lower pH value is appropriate for higher removal of Cr (VI) and the optimal pH occurred around pH 2–4 (99% removal). Then, with an increase in pH range from 7 to 8, the removal efficiencies and adsorption capacities decrease from 99 to 5.4% and 3 to 0.16 mg/g, respectively. This may be attributed to the reaction mechanism between the negatively charged dominant form of Cr (VI) and the positively charged functional groups of TBC-P at a lower pH, which is $HCrO_4^{2-}$. Similar findings were reported by Yao et al. and Babu and Gupta [34,35].

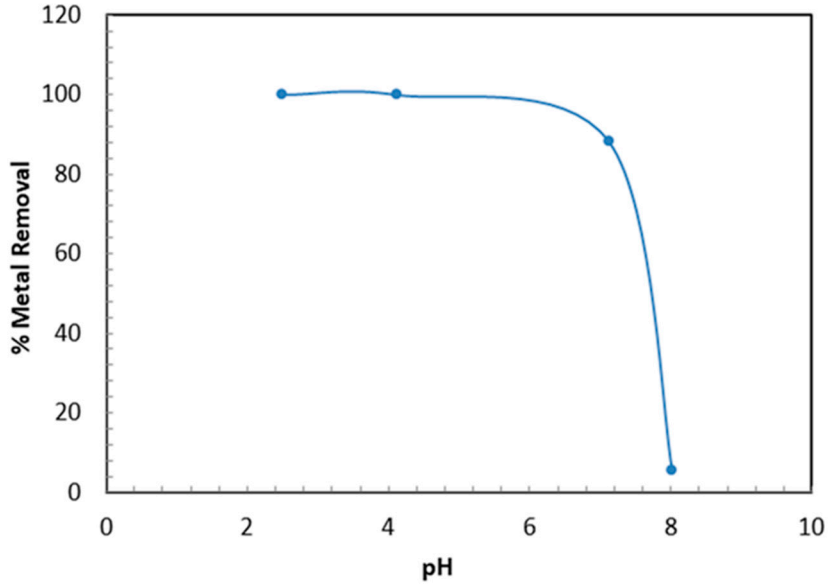

Figure 6. Influence of pH on the Cr (VI) removal by TBC-P.

3.2.3. Effect of TBC-P Dose on Cr (VI) Uptake

In order to identify the optimum dose of the TBC-P sample for maximizing the interactions among metal and active sites of adsorbent in the solution, different doses of the TBC-P (0.005–0.2 g) were added to 30 mL of metal solution (20 mg/L) at pH 2.0 and 25 °C for 24 h. The results are presented in Figure 7. Figure 7 demonstrates that with an increase in dose amount, the Cr (VI) removal efficiency increased while the adsorption capacity of TBC-P decreased. It is obvious that the metal removal is clearly raised from 53.2% to 99% by increasing the TBC-P dosage from 0.005 to 0.2 g. This is due to the increasing number of available adsorption sites as more adsorbent is added. However, it was found that the q_e decreased from 63.78 to 3.0 mg/g by increasing the TBC-P amount from 0.005 to 0.2 g. If the adsorbent amount increased by keeping the Cr (VI) concentration constant, the amount of Cr (VI) adsorbed per unit mass showed a decrease due to the availability of fewer Cr (VI) ions per unit mass of the TBC-P adsorbent. The drop in adsorption capacity is basically due to the sites remaining unsaturated during the adsorption process.

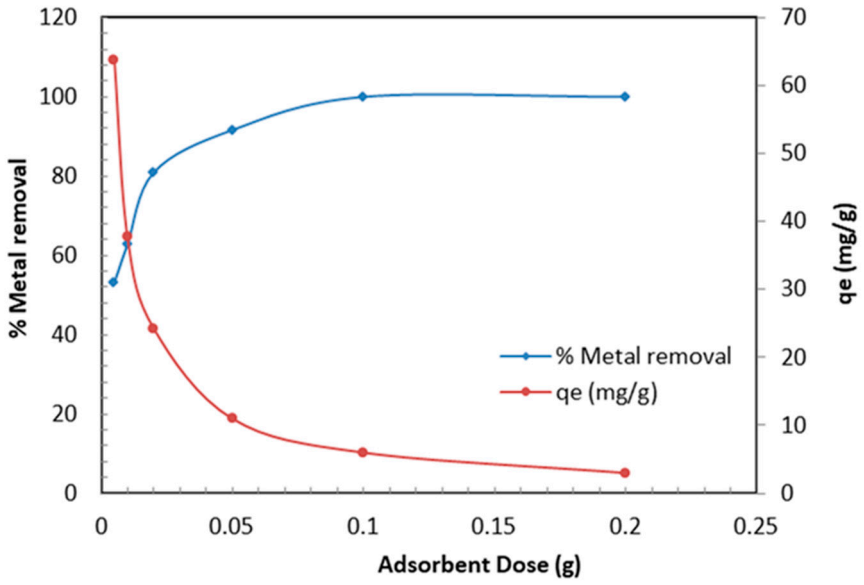

Figure 7. Effect of TBC-P dose on metal removal efficiency and adsorption capacity.

3.2.4. Influence of Metal Initial Concentration

Figure 8 shows the influence of various Cr (VI) concentrations on the metal removal efficiency of TBC-P. The concentration was changed from 10 to 250 mg/L at pH 2.0, 0.2 adsorbent dose and 25 °C for 24 h. Figure 8 displays that initially, when the concentration of the solution was low, i.e., 10, 20 and 40 mg/L, the metal removal efficiency was almost 100% and gradually decreased from 69.49% to 38.88% for 60 mg/L and 250 mg/L concentration levels, respectively. Therefore, a 0.2 g dose of UBC-P efficiently removed the concentration less than or equal to 40 mg/L of Cr (VI) and was considered the optimum concentration. The decrease in the metal removal efficiency was a result of the saturation of active sites with an increase in the metal concentration. Oppositely, the adsorption capacity increased (from 1.5 to 14.58 mg/g) when initial metal concentrations were increased from 10 to 250 mg/L. As a result, the number of attractive interactions between Cr (VI) and the TBC-P adsorbent increased. At a concentration increase, the concentration gradient was stronger and the adsorption capacity was higher [36].

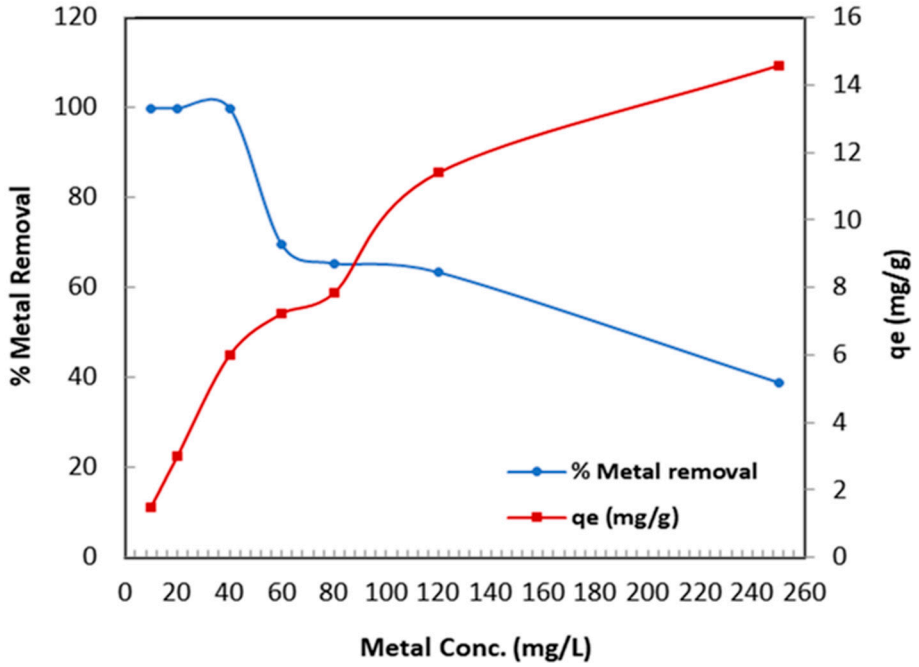

Figure 8. Influence of Cr (VI) metal ion concentration on metal removal and adsorption capacity.

3.2.5. Kinetics Analysis

The adsorption kinetic behavior of Cr (VI) onto TBC-P was studied using the pseudo-first- and second-order models. The coefficient of determination (R^2) was the base for selecting the best-fit model. The first-order equation is presented by the following Lagergren rate equation [37].

$$\ln(q_e - q_t) = \ln q_e - k_1 t \quad (3)$$

Similarly, the second-order equation is presented as [38]:

$$\frac{t}{q_t} = \frac{1}{k_2 q_e^2} + \frac{1}{q_e} t \quad (4)$$

where k_1 (min^{-1}) and k_2 (g/mg·min) are the rate constants of the first- and second-order kinetic models, respectively, and t is the time (min).

The correlation coefficient and the constants obtained for the kinetic models are summarized in Table 3; the plot of the linearized form of Equations (3) and (4) for TBC-P adsorbent is shown in Figure 9. The modeling outcomes specify that the Cr (VI) sorption onto TBC-P was well presented by the second-order kinetic model with R^2 (0.9991). How-

ever, the pseudo-first-order showed a lower R^2 value (0.5103). In addition, there was a good agreement between the experimental value ($q_{e,cal}$ = 1.65) and the calculated value ($q_{e,exp}$ = 2.49) obtained from the second-order plot. A similar trend was found for the Cr (VI) uptake on chitin, chitosan, *Rhizopus arrhizus* and a bio-composite of mango by Babu and Gupta and Sağ and Aktay [34,39].

Table 3. Kinetic models constant parameters and correlation coefficient.

Model	Parameters	
	$q_{e,exp}$ (mg/g)	**2.49**
Pseudo-first-order	$q_{e,cal}$ (mg/g)	1.44
	k_1 (min^{-1})	0.0059
	R^2	0.5103
Pseudo-second-order	$q_{e,cal}$ (mg/g)	1.65
	k_2 (g/mg·min)	0.193
	R^2	0.9991

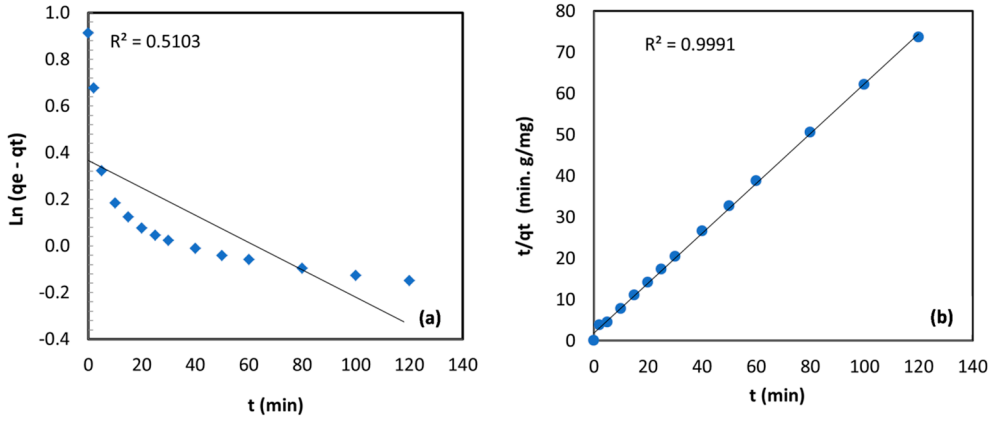

Figure 9. (**a**) First-order and (**b**) second-order kinetic models for metal adsorption onto TBC-P.

3.2.6. Isotherms Analysis

The Langmuir equation is presented as [40]:

$$\frac{C_e}{q_e} = \frac{1}{Q_{max}.b} + \frac{C_e}{Q_{max}} \quad (5)$$

where Q_{max} is the maximum adsorption capacity and b is the Langmuir constant (L/mg). Figure 10 displays the Cr (VI) Langmuir isotherm plots of Cr (VI) on TBC-P.

The Freundlich isotherm is presented as [41]:

$$\mathrm{Log}(q_e) = \mathrm{Log}(K_F) + \left(\frac{1}{n}\right)\mathrm{Log}(C_e) \quad (6)$$

where K_F (mg/g $(L/mg)^{1/n}$) and n are Freundlich constants. The parameters of the isotherm models and R^2 values are given in Table 4. In this work, the 1/n value is smaller than unity, specifying the favorable adsorption [41], and the Langmuir constants Q_{max} and b are found to be 14.97 mg/g and 0.102 L/mg, respectively (Table 4). The outcomes demonstrated that adsorption is best-fit in the Langmuir isotherm with R^2 = 0.96.

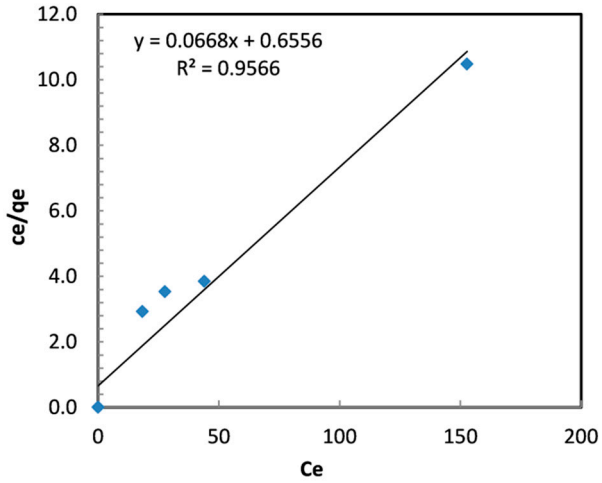

Figure 10. Langmuir isotherm plots for the removal of Cr (VI) by TBC-P.

Table 4. Isotherm model parameters.

T (°C)	Langmuir Isotherm			Freundlich Isotherm		
25	b (L/mg)	Q_{max} (mg/g)	R^2	1/n	K_F (mg/g (L/mg) $^{1/n}$)	R^2
	0.102	14.97	0.957	0.1684	5.296	0.779

3.2.7. Comparison of the Cr (VI) Adsorption Capacity with Literature

The Q_{max} of various adsorbents for Cr (VI) removal is compared in Table 5. As can be observed, the adsorption capacity of TBC-P is higher than many of the other modified as well as unmodified biochars. Moreover, the performance of TBC-P in this study is notably higher than that of previously analyzed sophora japonica Linn biochar, natural goethite, samanea saman activated carbon, activated clay mineral biochar composite, sagwan sawdust derived biochar and fungal biomass of Rhizopus sp. In addition, it can be observed that the optimum Cr (VI) removal can be achieved in the pH range of 2–5 (Table 5), which is applicable to the present study as well. Moreover, experimental conditions such as pH, temperature and initial adsorbate concentration are factors that influence the overall adsorption performance of the adsorbate. Though the studied biochar in this work had a fair adsorption capacity, it was lower than that of many other adsorbents, such as polyaniline-coated date seed-derived biochar, magnetic biochar derived from bagasse, pineapple peel-derived biochar and modified Lagerstroemia speciosa hull biochar.

Table 5. Comparison of the adsorption capacities of various adsorbents.

Adsorbents	Temperature (°C)	pH	C_0 (mg/g)	Q_{max} (mg/g)	References
Sophora japonica Linn biochar	25	2	5–400	9.58	[41]
Natural goethite	25	2	2–25	0.727	[42]
AC derived from the coconut shell	25	2	10–30	14.62	[43]
Samanea saman activated carbon	25	5	5–30	0.2893	[44]
Sagwan sawdust-derived biochar	25	2	30–100	9.62	[45]
Activated clay mineral biochar composite	25	3	1–11	6.84	[46]
Fungal biomass of Rhizopus sp.	25	2	12.5–300	8.06	[47]
TBC-P	25	2	10–250	14.97	This study
Polyaniline-coated date seed-derived biochar	50	5	2–100	27.3	[48]
Magnetic biochar derived from bagasse	25	2	5–300	29.08	[49]
Pineapple peel-derived biochar	25	2	10–500	23.81	[50]
H3PO4- modified Lagerstroemia speciosa hull biochar	30	2	25–100	41.92	[51]

3.2.8. Regeneration and Reusability of the TBC-P

The feasibility of using TBC-P in industrial applications also depends on the number of cycles that could be performed without compromising its sorption capacity and the ease of regeneration. In this work, desorption studies were conducted under optimal conditions obtained from adsorption studies in batch adsorption, where 0.2 g of TBC-P adsorbent was mixed with 30 mL of Cr (VI) with a concentration of 20 mg/L at pH 2 and room temperature for 24 h. Then, the spent TBC-P was collected and washed with a 0.1M HCl solution several times. After the HCl treatment, the TBC-P was separated from the solution and washed with distilled water until the pH of the wash effluent stabilized near 7.0. Regeneration and reuse studies were conducted for three cycles with the same adsorbent. The results displayed that there was a slight decrease in the Cr (VI) percentage of removal from 99% in the first cycle to 97.8% after the second cycle. Then, in the third cycle, the percentage of removal decreased to 93.7%. Thus, it can be deduced that TBC-P showed excellent regeneration ability in up to three recycling procedures, which indicated that TBC-P can be employed as an economically potential adsorbent.

4. Conclusions

In the present work, biochar derived from palm leaves was successfully modified with phosphoric acid and was used to remove Cr (VI) from an aqueous solution. It was noticed that the acid treatment of biochar by H_3PO_4 increased the metal sorption with respect to untreated biochar. This was basically due to the increase in surface area, oxygenated functional groups and development of acid-base surfaces that have important effects on the Cr (VI) adsorption. As a result, the treated biochar showed a much better sorption ability Cr (VI) than the untreated biochar, although the adsorbent dosage, initial solution of pH and initial metal concentration affected the removal rates. In general, the sorption of the Cr (VI) ions by the UBC-P increased with the increasing initial metal concentration and dose while decreasing at pH values beyond 4. The high uptake of Cr (VI) found in the initial pH varied from 2 to 4. The desorption of Cr (VI) from the TBC-P surface could be effectively carried out using a 0.1 M HCl solution. The regeneration efficiency was 99% in the first cycle and reduced to 93.7% in the third cycle. The adsorption mechanism was observed to be well described by the second-order model. The Langmuir isotherm best represented the adsorption data with Q_{max} (14.97 mg/g).

Funding: This work was supported by the Deanship of Scientific Research, Vice Presidency for Graduate Studies and Scientific Research, King Faisal University, Saudi Arabia (Grant No. 2423).

Data Availability Statement: Not applicable.

Acknowledgments: The author acknowledges the King Faisal University for facilitating laboratory works besides getting this work accomplished.

Conflicts of Interest: The author declares no conflict of interest.

References

1. Li, Y.; Gupta, R.; You, S. Machine learning assisted prediction of biochar yield and composition via pyrolysis of biomass. *Bioresour. Technol.* **2022**, *359*, 127511. [CrossRef] [PubMed]
2. Yrjälä, K.; Ramakrishnan, M.; Salo, E. Agricultural waste streams as resource in circular economy for biochar production towards carbon neutrality. *Curr. Opin. Environ. Sci. Health* **2022**, *26*, 100339. [CrossRef]
3. Mishra, R.K.; Kumar, D.J.; Narula, A.; Chistie, S.M.; Naik, S.U. Production and beneficial impact of biochar for environmental application: A review on types of feedstocks, chemical compositions, operating parameters, techno-economic study, and life cycle assessment. *Fuel* **2023**, *343*, 127968. [CrossRef]
4. Faiad, A.; Alsmari, M.; Ahmed, M.M.; Bouazizi, M.L.; Alzahrani, B.; Alrobei, H. Date palm tree waste recycling: Treatment and processing for potential engineering applications. *Sustainability* **2022**, *14*, 1134. [CrossRef]
5. Song, J.; He, Q.; Hu, X.; Zhang, W.; Wang, C.; Chen, R.; Wang, H.; Mosa, A. Highly efficient removal of Cr (VI) and Cu (II) by biochar derived from Artemisia argyi stem. *Environ. Sci. Pollut. Res.* **2019**, *26*, 13221–13234. [CrossRef]
6. Lakherwal, D. Adsorption of heavy metals: A review. *Int. J. Environ. Res. Dev.* **2014**, *4*, 41–48.

7. Mansoor, S.; Kour, N.; Manhas, S.; Zahid, S.; Wani, O.A.; Sharma, V.; Wijaya, L.; Alyemeni, M.N.; Alsahli, A.A.; El-Serehy, H.A.; et al. Biochar as a tool for effective management of drought and heavy metal toxicity. *Chemosphere* **2021**, *271*, 129458. [CrossRef]
8. Chattree, A.; Dan, S.; Jeyasundari, J.; Rathish, R.J.; Nguyen, T.A.; Rajendran, S. Detection and evaluation of trace metals in soil using nanosensors. In *Nanosensors for Smart Agriculture*; Elsevier: Amsterdam, The Netherlands, 2022; pp. 217–235.
9. Zhang, H.; Wang, J.; Zhou, B.; Zhou, Y.; Dai, Z.; Zhou, Q.; Chriestie, P.; Luo, Y. Enhanced adsorption of oxytetracycline to weathered microplastic polystyrene: Kinetics, isotherms and influencing factors. *Environ. Pollut.* **2018**, *243*, 1550–1557. [CrossRef]
10. Lee, D.J.; Cheng, Y.L.; Wong, R.J.; Wang, X.D. Adsorption removal of natural organic matters in waters using biochar. *Bioresour. Technol.* **2018**, *260*, 413–416. [CrossRef]
11. Burakov, A.E.; Galunin, E.V.; Burakova, I.V.; Kucherova, A.E.; Agarwal, S.; Tkachev, A.G.; Gupta, V.K. Adsorption of heavy metals on conventional and nanostructured materials for wastewater treatment purposes: A review. *Ecotoxicol. Environ. Saf.* **2018**, *148*, 702–712. [CrossRef]
12. Fan, Q.; Sun, J.; Chu, L.; Cui, L.; Quan, G.; Yan, J.; Hussain, Q.; Iqbal, M. Effects of chemical oxidation on surface oxygen-containing functional groups and adsorption behavior of biochar. *Chemosphere* **2018**, *207*, 33–40. [CrossRef] [PubMed]
13. Hu, X.J.; Liu, Y.G.; Wang, H.; Zeng, G.M.; Hu, X.; Guo, Y.M.; Li, T.T.; Chen, A.W.; Jiang, L.H.; Guo, F.Y. Adsorption of copper by magnetic graphene oxide-supported β-cyclodextrin: Effects of pH, ionic strength, background electrolytes, and citric acid. *Chem. Eng. Res. Des.* **2015**, *93*, 675–683. [CrossRef]
14. Puglla, E.P.; Guaya, D.; Tituana, C.; Osorio, F.; García-Ruiz, M.J. Biochar from agricultural by-products for the removal of lead and cadmium from drinking water. *Water* **2020**, *12*, 2933. [CrossRef]
15. Hussin, F.; Aroua, M.K.; Szlachta, M. Biochar derived from fruit by-products using pyrolysis process for the elimination of Pb (II) ion: An updated review. *Chemosphere* **2022**, *287*, 132250. [CrossRef] [PubMed]
16. Sireesha, S.; Upadhyay, U.; Sreedhar, I. Comparative studies of heavy metal removal from aqueous solution using novel biomass and biochar-based adsorbents: Characterization, process optimization, and regeneration. *Biomass Convers. Biorefinery* **2022**, 1–3. [CrossRef]
17. Rani, L.; Kaushal, J.; Lal Srivastav, A. Biochar as sustainable adsorbents for chromium ion removal from aqueous environment: A review. *Biomass Convers. Biorefinery* **2022**, 1–4. [CrossRef]
18. Sizmur, T.; Fresno, T.; Akgül, G.; Frost, H.; Moreno-Jiménez, E. Biochar modification to enhance sorption of inorganics from water. *Bioresour. Technol.* **2017**, *246*, 34–47. [CrossRef]
19. Zeng, H.; Zeng, H.; Zhang, H.; Shahab, A.; Zhang, K.; Lu, Y.; Nabi, I.; Naseem, F.; Ullah, H. Efficient adsorption of Cr (VI) from aqueous environments by phosphoric acid activated eucalyptus biochar. *J. Clean. Prod.* **2021**, *286*, 124964. [CrossRef]
20. Karim, A.A.; Kumar, M.; Mohapatra, S.; Panda, C.R.; Singh, A. Banana peduncle biochar: Characteristics and adsorption of hexavalent chromium from aqueous solution. *Methodology* **2014**, *7*, 1–10. [CrossRef]
21. Yin, W.; Guo, Z.; Zhao, C.; Xu, J. Removal of Cr (VI) from aqueous media by biochar derived from mixture biomass precursors of Acorus calamus Linn. and feather waste. *J. Anal. Appl. Pyrolysis* **2019**, *140*, 86–92. [CrossRef]
22. Yu, J.; Jiang, C.; Guan, Q.; Ning, P.; Gu, J.; Chen, Q.; Zhang, J.; Miao, R. Enhanced removal of Cr (VI) from aqueous solution by supported ZnO nanoparticles on biochar derived from waste water hyacinth. *Chemosphere* **2018**, *195*, 632–640. [CrossRef] [PubMed]
23. Han, Y.; Cao, X.; Ouyang, X.; Sohi, S.P.; Chen, J. Adsorption kinetics of magnetic biochar derived from peanut hull on removal of Cr (VI) from aqueous solution: Effects of production conditions and particle size. *Chemosphere* **2016**, *145*, 336–341. [CrossRef] [PubMed]
24. Shan, R.; Shi, Y.; Gu, J.; Bi, J.; Yuan, H.; Luo, B.; Chen, Y. Aqueous Cr (VI) removal by biochar derived from waste mangosteen shells: Role of pyrolysis and modification on its absorption process. *J. Environ. Chem. Eng.* **2020**, *8*, 103885. [CrossRef]
25. Zhang, X.; Lv, L.; Qin, Y.; Xu, M.; Jia, X.; Chen, Z. Removal of aqueous Cr (VI) by a magnetic biochar derived from Melia azedarach wood. *Bioresour. Technol.* **2018**, *256*, 1–10. [CrossRef] [PubMed]
26. Mathabatha, T.I.; Matheri, A.N.; Belaid, M. Peanut Shell-Derived Biochar as a Low-Cost Adsorbent to Extract Cadmium, Chromium, Lead, Copper, and Zinc (Heavy Metals) from Wastewater: Circular Economy Approach. *Circ. Econ. Sustain.* **2022**, 1–20. [CrossRef]
27. Zhao, N.; Zhao, C.; Lv, Y.; Zhang, W.; Du, Y.; Hao, Z.; Zhang, J. Adsorption and coadsorption mechanisms of Cr (VI) and organic contaminants on H3PO4 treated biochar. *Chemosphere* **2017**, *186*, 422–429. [CrossRef]
28. Pezoti, O.; Cazetta, A.L.; Bedin, K.C.; Souza, L.S.; Martins, A.C.; Silva, T.L.; Júnior, O.O.; Visentainer, J.V.; Almeida, V.C. NaOH-activated carbon of high surface area produced from guava seeds as a high-efficiency adsorbent for amoxicillin removal: Kinetic, isotherm and thermodynamic studies. *Chem. Eng. J.* **2016**, *288*, 778–788. [CrossRef]
29. Singh, B.; Camps-Arbestain, M.; Lehmann, J. (Eds.) *Biochar: A Guide to Analytical Methods*; Csiro Publishing: Clayton, Australia, 2017.
30. Peng, H.; Gao, P.; Chu, G.; Pan, B.; Peng, J.; Xing, B. Enhanced adsorption of Cu (II) and Cd (II) by phosphoric acid-modified biochars. *Environ. Pollut.* **2017**, *229*, 846–853. [CrossRef]
31. Sizirici, B.; Fseha, Y.H.; Yildiz, I.; Delclos, T.; Khaleel, A. The effect of pyrolysis temperature and feedstock on date palm waste derived biochar to remove single and multi-metals in aqueous solutions. *Sustain. Environ. Res.* **2021**, *31*, 9. [CrossRef]
32. Hossain, N.; Nizamuddin, S.; Griffin, G.; Selvakannan, P.; Mubarak, N.M.; Mahlia, T.M. Synthesis and characterization of rice husk biochar via hydrothermal carbonization for wastewater treatment and biofuel production. *Sci. Rep.* **2020**, *10*, 18851. [CrossRef]

33. Lowell, S.; Shields, J.E.; Thomas, M.A.; Thommes, M. *Characterization of Porous Solids and Powders: Surface Area, Pore Size and Density*; Springer Science & Business Media: Berlin/Heidelberg, Germany, 2006.
34. Babu, B.V.; Gupta, S. Adsorption of Cr (VI) using activated neem leaves: Kinetic studies. *Adsorption* **2008**, *14*, 85–92. [CrossRef]
35. Yao, Y.; Bing, H.; Feifei, X.; Xiaofeng, C. Equilibrium and kinetic studies of methyl orange adsorption on multiwalled carbon nanotubes. *Chem. Eng. J.* **2011**, *170*, 82–89. [CrossRef]
36. Morosanu, I.; Teodosiu, C.; Paduraru, C.; Ibanescu, D.; Tofan, L. Biosorption of lead ions from aqueous effluents by rapeseed biomass. *New Biotechnol.* **2017**, *39*, 110–124. [CrossRef]
37. Zhu, H.Y.; Jiang, R.; Xiao, L.; Zeng, G.M. Preparation, characterization, adsorption kinetics and thermodynamics of novel magnetic chitosan enwrapping nanosized γ-Fe2O3 and multi-walled carbon nanotubes with enhanced adsorption properties for methyl orange. *Bioresour. Technol.* **2010**, *101*, 5063–5069. [CrossRef] [PubMed]
38. Marcu, C.V.; Varodi, C.; Balla, A. Adsorption kinetics of chromium (VI) from aqueous solution using an anion exchange resin. *Anal. Lett.* **2021**, *54*, 140–149. [CrossRef]
39. Sağ, Y.; Aktay, Y. Kinetic studies on sorption of Cr (VI) and Cu (II) ions by chitin, chitosan and Rhizopus arrhizus. *Biochem. Eng. J.* **2002**, *12*, 143–153. [CrossRef]
40. Dehghani, M.H.; Sanaei, D.; Ali, I.; Bhatnagar, A. Removal of chromium (VI) from aqueous solution using treated waste newspaper as a low-cost adsorbent: Kinetic modeling and isotherm studies. *J. Mol. Liq.* **2016**, *215*, 671–679. [CrossRef]
41. Zhang, Q.C.; Wang, C.C.; Cheng, J.H.; Zhang, C.L.; Yao, J.J. Removal of Cr (VI) by biochar derived from six kinds of garden wastes: Isotherms and kinetics. *Materials* **2021**, *14*, 3243. [CrossRef]
42. Kar, S.; Equeenuddin, S.M. Adsorption of hexavalent chromium using natural goethite: Isotherm, thermodynamic and kinetic study. *J. Geol. Soc. India* **2019**, *93*, 285–292. [CrossRef]
43. Chandana, L.; Krushnamurty, K.; Suryakala, D.; Subrahmanyam, C. Low-cost adsorbent derived from the coconut shell for the removal of hexavalent chromium from aqueous medium. *Mater. Today Proc.* **2020**, *26*, 44–51. [CrossRef]
44. Niam, A.C.; Fenelon, E.; Ningsih, E.; Mirzayanti, Y.W.; Kristanti, E. High-efficiency adsorption of hexavalent chromium from aqueous solution by Samanea saman activated carbon. *Adsorpt. Sci. Technol.* **2022**, *2022*, 1–10. [CrossRef]
45. Gupta, G.K.; Mondal, M.K. Mechanism of Cr (VI) uptake onto sagwan sawdust derived biochar and statistical optimization via response surface methodology. *Biomass Convers. Biorefinery* **2023**, *13*, 709–725. [CrossRef]
46. Qhubu, M.C.; Mgidlana, L.G.; Madikizela, L.M.; Pakade, V.E. Preparation, characterization and application of activated clay biochar composite for removal of Cr (VI) in water: Isotherms, kinetics and thermodynamics. *Mater. Chem. Phys.* **2021**, *260*, 124165. [CrossRef]
47. Espinoza-Sanchez, M.A.; Arevalo-Nino, K.; Quintero-Zapata, I.; Castro-Gonzalez, I.; Almaguer-Cantu, V. Cr (VI) adsorption from aqueous solution by fungal bioremediation based using *Rhizopus* sp. *J. Environ. Manag.* **2019**, *251*, 109595. [CrossRef]
48. Tripathy, S.; Sahu, S.; Patel, R.K.; Panda, R.B.; Kar, P.K. Efficient removal of Cr (VI) by polyaniline modified biochar from date (*Phoenix dactylifera*) seed. *Groundw. Sustain. Dev.* **2021**, *15*, 100653. [CrossRef]
49. Liang, M.; Ding, Y.; Zhang, Q.; Wang, D.; Li, H.; Lu, L. Removal of aqueous Cr (VI) by magnetic biochar derived from bagasse. *Sci. Rep.* **2020**, *10*, 21473. [CrossRef]
50. Shakya, A.; Agarwal, T. Removal of Cr (VI) from water using pineapple peel derived biochars: Adsorption potential and re-usability assessment. *J. Mol. Liq.* **2019**, *293*, 111497. [CrossRef]
51. Nawaz, A.; Singh, B.; Kumar, P. H_3PO_4-modified Lagerstroemia speciosa seed hull biochar for toxic Cr (VI) removal: Isotherm, kinetics, and thermodynamic study. *Biomass Convers. Biorefinery* **2021**, 1–5. [CrossRef]